PHYSICAL REVIEW D **93,** 075004 (2016)

Status of the 98–125 GeV Higgs bosons scenario with updated LHC-8 data

Biplob Bhattacherjee,[1,*] Manimala Chakraborti,[2,†] Amit Chakraborty,[3,‡]
Utpal Chattopadhyay,[2,§] and Dilip Kumar Ghosh[2,‖]

[1]*Centre for High Energy Physics, Indian Institute of Science, Bangalore 560012, India*
[2]*Department of Theoretical Physics, Indian Association for the Cultivation of Science, 2A & B, Raja S.C. Mullick Road, Jadavpur, Kolkata 700 032, India*
[3]*Department of Theoretical Physics, Tata Institute of Fundamental Research, 1, Homi Bhabha Road, Mumbai 400005, India*

(Received 8 December 2015; published 5 April 2016)

In the context of the minimal supersymmetric standard model (MSSM), we discuss the possibility of the lightest Higgs boson with mass $M_h = 98$ GeV to be consistent with the 2.3σ excess observed at the LEP in the decay mode $e^+e^- \to Zh$, with $h \to b\bar{b}$. In the same region of the MSSM parameter space, the heavier Higgs boson (H) with mass $M_H \sim 125$ GeV is required to be consistent with the latest data on Higgs coupling measurements at the end of the $7 + 8$ TeV LHC run with 25 fb^{-1} of data. While scanning the MSSM parameter space, we impose constraints coming from flavor physics, relic density of the cold dark matter as well as direct dark matter searches. We study the possibility of observing this light Higgs boson in vector boson fusion process and associated production with W/Z-boson at the high luminosity (3000 fb^{-1}) run of the 14 TeV LHC. Our analysis shows that this scenario can hardly be ruled out even at the high luminosity run of the LHC. However, the precise measurement of the Higgs signal strength ratios can play a major role to distinguish this scenario from the canonical MSSM one.

DOI: 10.1103/PhysRevD.93.075004

I. INTRODUCTION

The LHC has recently started its second phase of run. The discovery of a new scalar particle of mass ∼125 GeV has been confirmed [1]. The properties of this newly discovered resonance seem to be in close agreement with that of the Standard Model (SM) Higgs boson of the same mass [2]. The production modes for the Higgs boson at the LHC are those via the gluon-gluon fusion, the vector boson $(W^{\pm}, Z)$ fusion, and the associated production with a vector boson $(W^{\pm}, Z)$ or top quarks whereas its most effective decay modes are into four leptons (e and μ), W^+W^{*-}, and $\gamma\gamma$ channels. One of the main goals of the current LHC run with increased center of mass energy and higher luminosity is to find out whether the discovered particle is the Standard Model Higgs boson or a part of an extended Higgs sector containing several other physical scalars.

The Higgs sector of the minimal supersymmetric Standard Model (MSSM) [3–6] has a far richer spectrum than that of the SM. The model has two CP-even neutral scalars (the lighter and the heavier ones h and H respectively), one CP-odd neutral scalar (A), and two charged scalars ($H^{\pm}$). At the tree level, only two input parameters other than the Z-boson mass (M_Z) are required to specify the Higgs sector of the MSSM. These inputs are (i) the mass of the pseudoscalar Higgs boson (M_A) and (ii) the ratio of vacuum expectation values (vevs) of the two Higgs doublets of the MSSM ($\tan\beta$). Dependence on other input parameters are induced once the radiative corrections to the Higgs mass are taken into account. We note that the couplings of H to the gauge bosons such as HZZ, HW^+W^- are proportional to $\cos(\beta - \alpha)$ where α is the Higgs mixing angle [6]. On the other hand, couplings like hZZ, hW^+W^- are proportional to $\sin(\beta - \alpha)$.

In the well-known decoupling limit of the MSSM[6] characterized by the mass hierarchy $M_H \simeq M_A \simeq M_{H^{\pm}} \gg M_Z$, M_h, all the Higgs bosons become much heavier than the lightest one (h) making the latter to have SM-like mass as well as couplings. In this limit one has $\cos(\beta - \alpha) \to 0$ indicating negligibly small values for the aforesaid couplings of the heavier Higgs bosons. Thus, it seems natural to consider the Higgs particle observed at the LHC as the lightest CP-even Higgs of the MSSM in the decoupling limit. However, the other possibility of having a nondecoupling regime of the MSSM where the observed boson at 125 GeV is interpreted as the heavier CP-even Higgs scalar H can be consistent with the nondecoupling regime of the MSSM Higgs bosons where $M_h \sim M_H \sim M_A \sim M_Z$ [6]. In this case, all the MSSM Higgses would be light with the lightest one lying somewhat below 125 GeV. The above nondecoupling scenario may get its motivation from an old result by the LEP Collaboration which corresponds to an excess of Higgs-like events around a mass of 98 GeV [7,8]. The excess was found in the channel $e^+e^- \to Zh$ with h

*biplob@cts.iisc.ernet.in
†tpmc@iacs.res.in
‡amit@theory.tifr.res.in
§tpuc@iacs.res.in
‖tpdkg@iacs.res.in

decaying into $b\bar{b}$. In a combined analysis of the four LEP working groups, this excess reached a significance of 2.3σ. The above phenomena cannot be explained within the SM since the SM Higgs boson would give rise to a larger production cross section. In our previous analysis of Ref. [9] we explored the possibility of interpreting the 2.3σ excess events in the MSSM with the name "Inclusive LEP-LHC Higgs (ILLH) scenario" where h and H are required to correspond to the LEP excess near 98 GeV and the observed resonance at ∼125 GeV at the LHC, respectively. There have been several studies in this direction and a partial list may be seen in Refs. [10–24]. In spite of the fact that the above MSSM scenario is believed to be cornered in recent times [25], we believe that it is important to review the current status of the scenario in relation to the latest LHC data via focusing our attention in relevant zones of appropriate parameters of MSSM in a model-independent way.

We must note that if this scenario is indeed realized then (i) the value of $\sin^2(\beta-\alpha)$ must be very small in order to explain the small ZZh coupling at LEP and (ii) the couplings of H must be similar to that of the SM Higgs in order to be compatible with the 125 GeV resonance observed at the LHC. The parameter region which satisfies these two requirements must also pass through other direct constraints coming from the LHC, the most important ones are given as below.

(i) Exclusion limits in the channel $H/A \to \tau^+\tau^-$: Both the ATLAS and CMS Collaborations have searched for a neutral Higgs-like boson Φ in the decay channel $\tau^+\tau^-$ for certain benchmark scenarios [26,27]. However, in order to perform a model-independent analysis one must consider the bounds on $\sigma \times \mathrm{BR}(\Phi \to \tau^+\tau^-)$ as a function of m_Φ, where σ denotes the production cross section for the non-minimal Higgs boson Φ decaying into the di-tau channel. Two different production modes for Φ are considered, namely, the gluon-gluon fusion and the associated production with b-quark.

(ii) Searches for $H^\pm$: The ATLAS and CMS searches for $H^\pm$ are performed in $t\bar{t}$ events with subsequent decays, $t \to bH^\pm$ and $H^\pm \to \tau\nu$ [28,29]. Model-independent upper bounds are obtained for $\mathrm{BR}(t \to bH^\pm) \times \mathrm{BR}(H^\pm \to \tau\nu)$. These searches exclude $\tan\beta$ up to 6 for 90 GeV $< M_{H^\pm} <$ 150 GeV.

These two searches together restrict $\tan\beta$ to have a very narrow range. Moreover, the constraints from heavy flavor physics also become very important in this region of parameter space. In particular, experimental limits on $\mathrm{BR}(b \to s\gamma)$ and $\mathrm{BR}(B_s \to \mu^+\mu^-)$ are able to play very crucial roles to constrain the MSSM parameter space under question.

In Ref. [9] we imposed all of the above bounds on the MSSM parameter space to probe whether it could accommodate the ILLH scenario. However, for the Higgs signal strength constraints we used a conservative lower bound on $\mu_{gg}^{\gamma\gamma}$ [see Eq. (3)] taken as $\mu_{gg}^{\gamma\gamma} > 0.5$. Afterwards, the bounds from the ATLAS and CMS Collaborations for the pseudoscalar and charged Higgs search channels have become more stringent. On the other hand, the Higgs signal strength results have become more precise in recent times. Thus, it seems very reasonable to reanalyze the 98–125 GeV Higgs scenario in the light of the updated collider constraints and to check whether there is any room left in the MSSM framework to accommodate a 98 GeV Higgs boson.

In this work we perform a detailed scan over the MSSM parameter space to find out the region allowed by all the relevant collider constraints mentioned above. We also demand that the MSSM parameter space must satisfy the PLANCK limit on dark matter (DM) relic density. Keeping these issues in mind we explore the possibility of observing the signals of the ILLH scenario in the high-luminosity (HL) run of the LHC. The plan of this paper is as follows.

In Sec. II we discuss the major constraints imposed on the MSSM parameter space of our interest and the parameter ranges we choose to perform the scanning procedure. The impact of the constraints on the MSSM parameter space as well as the main features of the allowed zone are studied in Sec. III. In Sec. IV we analyze the prospects of the ILLH scenario in the high-luminosity run of the LHC. Finally, we conclude in Sec. V.

II. RELEVANT CONSTRAINTS AND PARAMETER SPACE SCANNING

In this section we enumerate the essential constraints and the scanning details of the MSSM parameter space considered in this analysis.

A. The basic constraints for the ILLH scenario

The ILLH scenario requires that the lightest CP-even Higgs boson should have a mass around 98 GeV, while the one observed at the LHC at 125 GeV to be the heavier CP-even Higgs boson. Thus, we consider the following ranges for M_h and M_H:

$$95\ \mathrm{GeV} < M_h < 101\ \mathrm{GeV},$$
$$122\ \mathrm{GeV} < M_H < 128\ \mathrm{GeV}. \quad (1)$$

An uncertainty of 3 GeV in the Higgs boson mass is assumed which may come from the top mass uncertainty, uncertainties in the renormalization scheme, and higher order loop corrections [30]. The value of $\sin^2(\beta-\alpha)$ must lie within the following range in order to satisfy the LEP limit:

$$0.1 < \sin^2(\beta-\alpha) < 0.25. \quad (2)$$

B. Constraints from the LHC

The different production mechanisms of the Standard Model Higgs boson at the LHC are the gluon-gluon fusion (ggF), vector boson fusion (VBF), and associated production with gauge bosons (VH, $V = W^{\pm}, Z$) or with a pair of top quarks ($t\bar{t}H$). Among its various possible decay modes, the decay into a pair of bottom quarks is the most dominant one. Other subdominant decay modes include final states involving a pair of SM gauge bosons (VV^*), $\tau^+\tau^-$, and $\gamma\gamma$ etc. The di-photon final states refer to loop-induced phenomena involving W-boson and heavy fermion loops. Both the ATLAS and CMS Collaborations have analyzed various production and decay modes of the Higgs boson observed at 125 GeV and put bounds on the various couplings of the SM Higgs. The signal strength parameter μ is defined as the ratio between the measured Higgs boson rate and its SM expectation as follows:

$$\mu_i^f = \frac{\sigma_i \times \mathrm{BR}^f}{(\sigma_i)_{\mathrm{SM}} \times (\mathrm{BR}^f)_{\mathrm{SM}}}. \tag{3}$$

Here, σ_i represents the production cross section for a given new physics model with $i =$ ggF, VBF, VH, and $t\bar{t}H$ processes for a generic Higgs boson H with $f = \gamma\gamma$, ZZ^*, WW^*, $b\bar{b}$, $\tau^+\tau^-$ being the decay modes of the Higgs boson. The subscript "SM" represents the respective SM expectations. In Table I, we display the most updated combined results on various Higgs signal strengths by the ATLAS and CMS Collaborations [31]. The subscript F denotes the combined data for the ggF and $t\bar{t}H$ process, while V signifies the combined VBF and VH processes. Even though the Higgs production through the "fusion" (F) mode includes both the ggF and $t\bar{t}H$ processes, here we consider the ggF process only since $\frac{\sigma_{t\bar{t}H}}{\sigma_{ggF}} \sim 2\%$ as estimated by the combined ATLAS and CMS data and also uncertainties in Higgs signal strength measurements associated to the $t\bar{t}H$ process being relatively large. At the end of 8 TeV run of the LHC, the signal strength variables associated with the observed 125 GeV Higgs boson still allow significant deviations from the SM predictions. Keeping this in mind, here we consider 2σ deviations from the central value of various signal strength variables obtained after combining the ATLAS and CMS data.

TABLE I. Combined results of the Higgs coupling measurements by the ATLAS and CMS Collaborations at the end of the $7 + 8$ TeV run of the LHC with approximately 25 fb^{-1} of data [31].

Channel	Combined ATLAS + CMS Signal Strength
$\mu_F^{\gamma\gamma}$	$1.19^{+0.28}_{-0.25}$
μ_F^{WW}	$1.0^{+0.23}_{-0.20}$
μ_F^{ZZ}	$1.44^{+0.38}_{-0.34}$
μ_F^{bb}	$1.09^{+0.93}_{-0.89}$
$\mu_F^{\tau\tau}$	$1.10^{+0.61}_{-0.58}$
$\mu_V^{\gamma\gamma}$	$1.05^{+0.44}_{-0.41}$
μ_V^{WW}	$1.38^{+0.41}_{-0.37}$
μ_V^{ZZ}	$0.48^{+1.37}_{-0.91}$
μ_V^{bb}	$0.65^{+0.30}_{-0.29}$
$\mu_V^{\tau\tau}$	$1.12^{+0.37}_{-0.35}$

$$\begin{aligned} 0.69 < \mu_F^{\gamma\gamma} < 1.75, \quad & 0.6 < \mu_F^{WW} < 1.46, \quad & 0.76 < \mu_F^{ZZ} < 2.2, \\ -0.69 < \mu_F^{bb} < 2.95, \quad & -0.06 < \mu_F^{\tau\tau} < 2.32, \quad & 0.23 < \mu_V^{\gamma\gamma} < 1.93, \\ 0.64 < \mu_V^{WW} < 2.2, \quad & -1.34 < \mu_V^{ZZ} < 3.22, \quad & 0.07 < \mu_V^{bb} < 1.25, \\ & & 0.42 < \mu_V^{\tau\tau} < 1.86. \end{aligned} \tag{4}$$

Apart from the above, there are two experimental constraints that play crucial roles in the parameter space of our interest, namely, the limits from direct searches of the pseudoscalar and charged Higgs bosons at the LHC. We note that from the direct searches of the pseudoscalar Higgs boson, both the ATLAS and CMS Collaborations have eliminated the zone $90 < M_A < 250$ GeV for $\beta \gtrsim 5.5$ [26,27]. On the other hand, the ATLAS and CMS have also searched for light charged Higgs bosons using $t\bar{t}$ events via the $t \to bH^+$ mode with $H^+ \to \tau^+\nu_\tau$ [28,29]. The ATLAS analysis indicates that the regions of parameter space with $\tan\beta$ between 2 to 6 with $90 < m_{H^+} < 150$ GeV is disallowed. We note that the ATLAS and CMS exclusion limits are available for a few benchmark scenarios with specific choices of the MSSM model parameters (e.g., the so-called m_h^{max}, $m_h^{\mathrm{mod}\pm}$ etc. scenarios [26–29]). However, these scenarios seem to be rather over-simplified. On the other hand, there exist model-independent limits on the production cross-section times branching ratio, i.e., $\sigma \times \mathrm{BR}(\Phi \to \tau^+\tau^-)$, for a nonstandard Higgs boson Φ when it is produced via gluon-gluon fusion and b-quark associated processes [26,27]. We use these model-independent limits in the present work.

C. Constraints from flavor physics and cosmological abundance of dark matter

The light pseudoscalar and charged Higgs bosons naturally make the flavor physics constraints very significant for the parameter space of our interest. We consider the two most stringent rare b-decay constraints, namely, $\mathrm{BR}(b \to s\gamma)$ and $\mathrm{BR}(B_s \to \mu^+\mu^-)$, and allow 2σ deviation from the central limit[1] [32],

$$2.82 \times 10^{-4} < \mathrm{BR}(b \to s\gamma) < 4.04 \times 10^{-4}, \quad (5)$$

$$1.57 \times 10^{-9} < \mathrm{BR}(B_s \to \mu^+\mu^-) < 4.63 \times 10^{-9}. \quad (6)$$

Following the analysis of the PLANCK experiment [34] as in Ref. [9], we take the DM relic density limits as $0.112 < \Omega h^2 < 0.128$. However, in this analysis we allow the possibility of having a multicomponent DM scenario. Hence, we consider only the upper limit of the relic density constraint as given below.

$$\Omega_{\tilde{\chi}_1^0} h^2 < 0.128. \quad (7)$$

This allows for the possibility of an under-abundant DM scenario with relic density lying below the lower limit of the PLANCK data. We also check the consistency with the upper bounds on the DM direct detection cross section from the LUX [35] experiment.

D. Exploring the relevant MSSM parameter space for the ILLH scenario

Considering the data from $A/H \to \tau^+\tau^-$ and $H^+ \to \tau^+\nu_\tau$ search channels as constraints, we focus on the ILLH scenario for a small range of $\tan\beta$, namely, $1 < \tan\beta < 6.5$. Note that, LEP data [8] disfavors the region with $\tan\beta < 3$ for the SM-like SUSY Higgs boson search with the supersymmetry (SUSY) breaking scale $M_{\mathrm{SUSY}} = 1$ TeV. However, for a 98 GeV non-SM-like Higgs boson h, $\tan\beta$ can indeed be smaller than 3. Thus, in our analysis we probe the regions with smaller values of $\tan\beta$. On the other hand, the choice of a model-independent approach for Higgs mass motivates us for scanning up to $\tan\beta = 6.5$, a value higher than the limit of the ATLAS and CMS data.

We choose the decoupling zone (∼3 TeV) for the first two generations of squarks and sleptons, considering the fact that there is no effect on the Higgs spectra in phenomenological MSSM of the above scalars [36].

The parameter range over which we perform the random scan can be listed as follows:

$$\begin{aligned}
&1 < \tan\beta < 6.5, \qquad 0.12 < M_A < 0.3 \text{ TeV}, \qquad 0.3 \text{ TeV} < \mu < 12 \text{ TeV}^2 \\
&0.05 \text{ TeV} < M_1, \qquad M_2 < 1.5 \text{ TeV}, \qquad 0.5 \text{ TeV} < M_3 < 3 \text{ TeV}, \\
&-8 \text{ TeV} < A_t, \qquad A_b < 12 \text{ TeV}, \qquad A_u = A_d = A_\tau = A_e = 0, \\
&0.3 \text{ TeV} < M_{\tilde{q}_3} < 5 \text{ TeV}, \quad \text{where, } \tilde{q}_3 \equiv \tilde{t}_L, \tilde{t}_R, \tilde{b}_L, \tilde{b}_R \\
&M_{\tilde{q}_i} = 3 \text{ TeV}, \quad \text{for } i = 1,2 \quad \text{and} \quad M_{\tilde{l}_i} = 3 \text{ TeV}, \quad \text{for } i = 1,2,3.
\end{aligned} \quad (8)$$

[2] The relevant SM parameters are chosen as $m_b^{\overline{\mathrm{MS}}}(m_b) = 4.19$ GeV and $m_t^{\mathrm{pole}} = 173.3 \pm 2.8$ GeV (a larger error amount is considered following the argument of Ref. [37]) and the strong coupling constant $\alpha_s(M_Z) = 0.1172$. The stringency of satisfying Eq. (1) to Eq. (7) or primarily Eq. (1) and Eq. (2) requires a very dense parameter scan. In this work, the number of parameter points scanned is more than 80 million over the above ranges.

The publicly available code SuSpect (version 2.43) [38] is used for spectrum generation and micrOmegas (version 3.6.9.2) [39] is used for calculating the relic density and flavor observables while the branching ratios of the Higgs bosons are computed via HDECAY [40]. We calculate the Higgs production cross section using SuShi [41]. The lower limits on the sparticle masses are imposed from the LEP and LHC data. We consider the lightest top and bottom squark masses are greater than 500 GeV, while the gluinos are assumed to be heavier than 1.4 TeV [42]. We also impose the LEP limit on the lightest chargino mass to be 100 GeV [42]. The charge color breaking (CCB) constraints are already imposed by SuSpect while scanning the parameter space.[3]

[1] The current measurements of these two b-observables stand at $\mathrm{BR}(B_s \to X_s\gamma) = 3.43 \pm 0.22 \pm 0.21(\text{theo.})$ and $\mathrm{BR}(B_s \to \mu^+\mu^-) = 3.1 \pm 0.7 \pm 0.31(\text{theo.})$ [32]. We follow Ref. [33] for the conservative estimates of the theoretical uncertainties associated with these two flavor observables.

[2] In our quest to explore the validity of the ILLH scenario, we include large values μ in our parameter scan, keeping aside any fine-tuning related concern.

[3] Since the parameter ranges are associated with large values of μ and A_t, we have further used a more dedicated check for the CCB constraints by using the code Vevacious (version 1.1.3)[43] for the two chosen benchmark points (BPs) (see Sec. III). The code can check cosmological stability in presence of a CCB vacuum via using the code CosmoTransitions [44]. See Ref. [45] and references therein for further details.

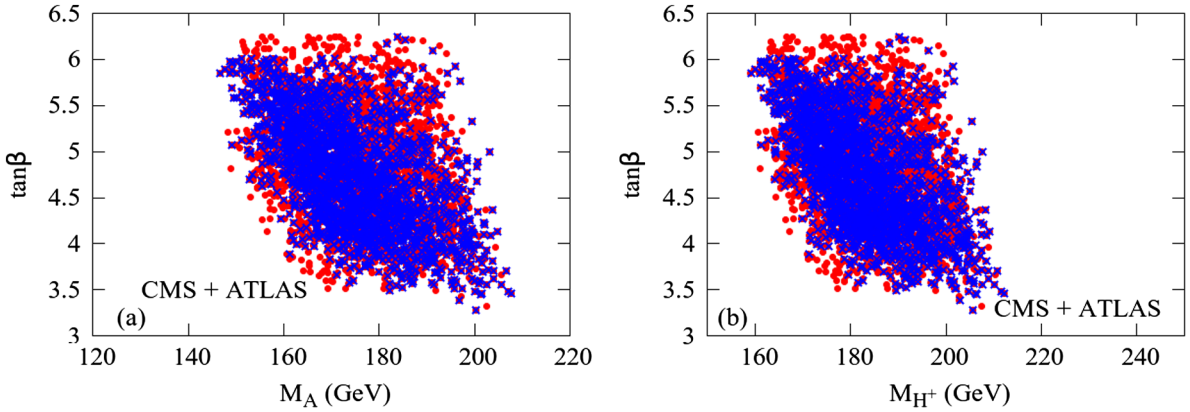

FIG. 1. Scatter plot in the $M_A - \tan\beta$ (left) and $M_{H^\pm} - \tan\beta$ (right) plane. The red circles represent the points which satisfy all the constraints [Eqs. (1)–(6)], while blue crosses display points which, in addition, satisfies the DM relic density constraint of Eq. (7).

III. RESULT

In Fig. 1, we display the allowed parameter space in the $M_A - \tan\beta$ and $M_{H^\pm} - \tan\beta$ planes, where the red circles represent the points which satisfy all the constraints [Eqs. (1)–(6)], except Eq. (7), while blue crossed points satisfy Eq. (7).

In Fig. 2, we show the distribution of $\sigma \times \mathrm{BR}(\Phi \to \tau^+\tau^-)$ where $\Phi \equiv h, A$, with respect to M_h and M_A for all the red circled points corresponding to Fig. 1, i.e., for those points which satisfy all the constraints [Eqs. (1)–(6)] except Eq. (7). The black solid and blue dashed lines represent the CMS and ATLAS bounds, respectively. The ggF

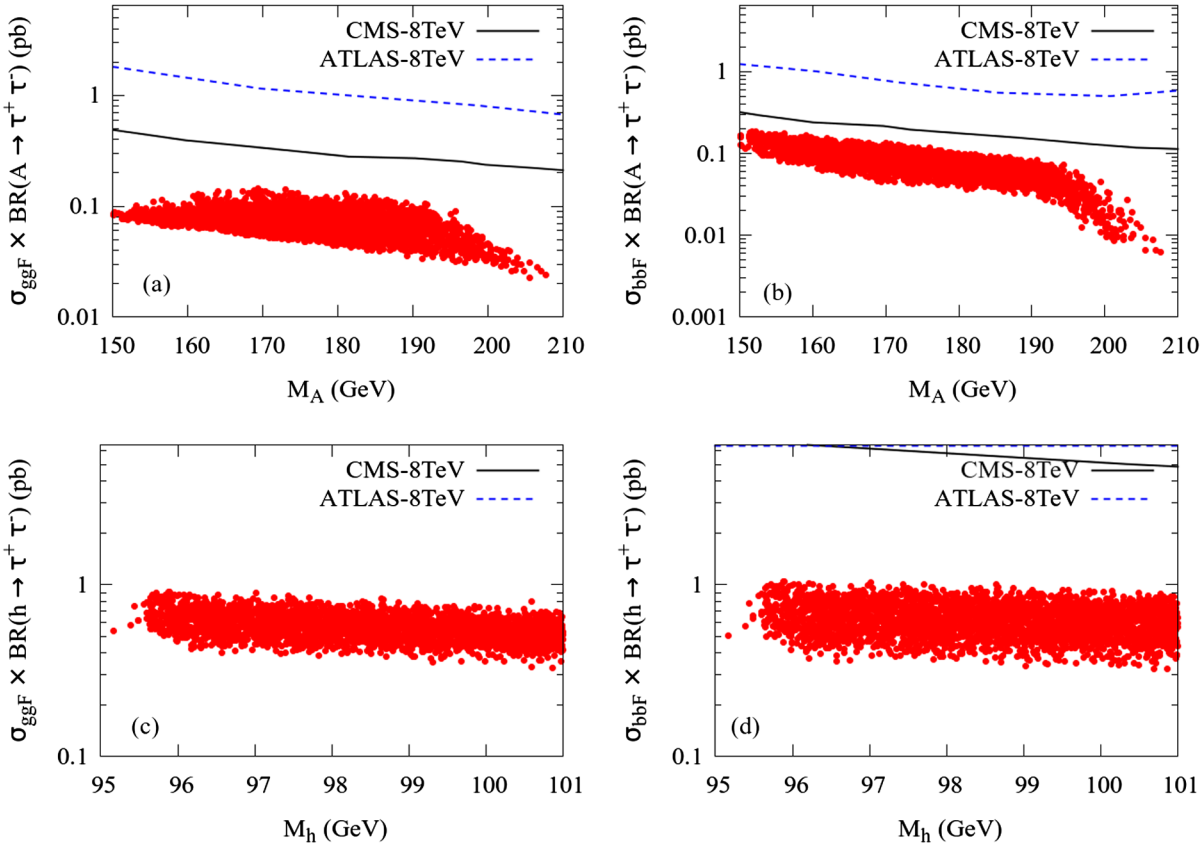

FIG. 2. Distribution of $\sigma \times \mathrm{BR}(\Phi \to \tau^+\tau^-)$ for all the red circled points corresponding to Fig. 1, i.e., for those points which satisfy all the constraints [Eq. (1)–(6)] except the relic density bound of Eq. (7). The black solid and blue dashed lines represent the CMS and ATLAS upper limits on this quantity. The upper and lower plots in the left panel assume Higgs is produced via ggF process, while bbF production mechanism is considered in the right panel. For details see text.

production cross section for both h and A increases with a decrease of $\tan\beta$. However, the branching ratio of h, $A \to \tau^+\tau^-$ also gets reduced as $\tan\beta$ decreases. Thus, for low values of $\tan\beta$ as in the region of our interest, the product $\sigma(ggF) \times \mathrm{BR}(\Phi \to \tau^+\tau^-)$ is still below the present experimental sensitivity, as can be seen from the left figures of both the upper and lower panels. However, when one considers the production mode of the Higgs boson in association with $b\bar{b}$, interestingly the present exclusion bounds are found to be very close to the model predictions. A better sensitivity in the $b\bar{b}$-fusion channel results in strong bounds on our parameter space. A sudden fall in $\sigma \times \mathrm{BR}(\Phi \to \tau^+\tau^-)$ distribution near $M_\phi = 190$ GeV originates from the opening of the dominant decay mode $A \to Zh$ ($m_h \sim 98$ GeV in our case) and consequent strong reduction in the branching ratio of $\Phi \to \tau^+\tau^-$. Thus, a closer look at these distributions reveals that one or two orders of improvement in the measurement of the quantity $\sigma \times \mathrm{BR}(\Phi \to \tau^+\tau^-)$ for both the production processes will put a strong constraint on the ILLH parameter space.

The allowed points in the present scenario correspond to the charged Higgs boson mass lying in the range 160–200 GeV. Thus, the dominant decay modes are seen to be $H^\pm \to \tau\nu_\tau$ and/or $H^\pm \to t\bar{b}$. Both the ATLAS and CMS Collaborations have performed searches for the charged Higgs bosons with masses larger than that of the top quark [46,47]. We find that the low $\tan\beta$ region with $M_{H^\pm} \geq 175$ GeV is consistent with the current LHC data.

A. Light charged Higgs bosons and flavor data

Flavor observables play a crucial role in determining the valid regions of the MSSM parameter space. For example, rare B-decays that are helicity suppressed within the SM may on the other hand receive large contributions from the loop corrections involving SUSY particles. Two such rare B-decays are the radiative decay $\mathrm{BR}(b \to s\gamma)$ and the pure leptonic decay $\mathrm{BR}(B_s \to \mu^+\mu^-)$. We will outline the relevant points of these constraints pertaining to our scenario with light $H^\pm$ while having large μ and a large third generation of trilinear coupling parameters. We will particularly focus on the features of the valid parameter zones as allowed by the above constraints. In our analysis with positive μ and gluino mass ($M_{\tilde{g}}$) it turns out that the valid zones also have positive A_t. This may be seen in the A_t-μ plot of Fig. 3. The red circles represent the points which satisfy all the constraints of Eq. (1) to (6), while blue crosses indicate parameter points that additionally satisfy the DM relic density constraint of Eq. (7).

The experimental data of $\mathrm{BR}(b \to s\gamma)$ leaves a very small room for any beyond the Standard Model contribution. SUSY scenarios are effectively constrained by $\mathrm{BR}(b \to s\gamma)$ (which has both an upper and a lower limit) due to cancellation of relevant diagrams, when the individual SUSY contributions may become large. However,

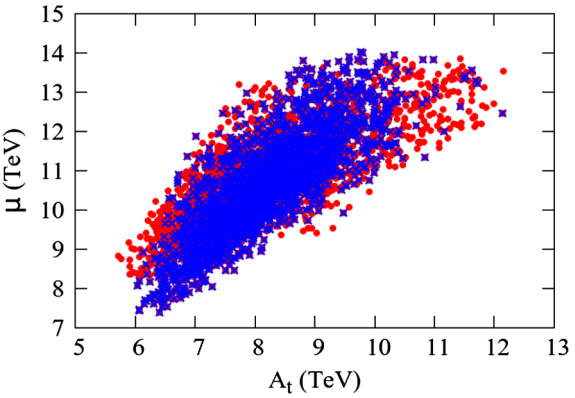

FIG. 3. Plot in A_t-μ plane. The symbols carry the same meaning as in Fig. 1.

we will see the importance of next-to-leading order (NLO) contributions in regard to this constraint. In the SM, the $t - W$ loops cause nonzero contributions to $\mathrm{BR}(b \to s\gamma)$, almost saturating the experimental value. In the MSSM, the dominant contributions to $\mathrm{BR}(b \to s\gamma)$ come from the $t - H^\pm$ and $\tilde{t}_{1,2} - \tilde{\chi}^\pm_{1,2}$ loops [48,49], where the former types of loops comes with the same sign with that of the $t - W$ loops of the SM. Considering the contributions of ${\tilde{\chi}_1}^\pm - \tilde{t}_1$ loops one has [50]

$$\mathrm{BR}(b \to s\gamma)|_{\chi^\pm} \propto \mu A_t \tan\beta f(m_{\tilde{t}_1}, m_{\tilde{t}_2}, m_{\tilde{\chi}^+}) \frac{m_b}{v(1+\Delta m_b)}. \tag{9}$$

On the other hand, for the $t - H^\pm$ loop contributions one finds [50]

$$\mathrm{BR}(b \to s\gamma)|_{H^+} \propto \frac{(h_t \cos\beta - \delta h_t \sin\beta)}{v\cos\beta} g(m_{H^+}, m_t) \times \frac{m_b}{(1+\Delta m_b)}. \tag{10}$$

Here f and g of Eqs. (9) and (10) are the loop functions. Δm_b refers to the SUSY corrections to bottom mass where the SUSY QCD (SQCD) corrections may have a significant role which we will discuss soon. δh_t, as appearing in the second term of Eq. (10), principally results from the corrections to the top quark Yukawa coupling due to SQCD effects and this gives rise to a NLO effect in $\mathrm{BR}(b \to s\gamma)$. The dominant SQCD corrections to δh_t arising from the gluino-squark loops are given by [50]

$$\delta h_t = h_t \frac{2\alpha_s}{3\pi} \mu M_{\tilde{g}} (\cos^2\theta_{\tilde{t}} I(m_{\tilde{s}_L}, m_{\tilde{t}_2}, M_{\tilde{g}}) + \sin^2\theta_{\tilde{t}} I(m_{\tilde{s}_L}, m_{\tilde{t}_1}, M_{\tilde{g}})), \tag{11}$$

where I is again a loop function and $\theta_{\tilde{t}}$ is the squark mixing angle for the third generation.

Coming to the SQCD corrections to Δm_b[4] we have two types of contributions, namely, from the $b-\tilde{g}$ and $\tilde{\chi}_1^{\pm}-t$ loops [51–55]. Following Ref. [52] the corrections are given as below.

$$\Delta m_b \simeq \frac{2\alpha_s}{3\pi} M_{\tilde{g}}(\mu \tan\beta - A_b) I(m_{\tilde{b}_1}, m_{\tilde{b}_2}, M_{\tilde{g}}) + \frac{h_t^2}{16\pi^2}\mu(A_t \tan\beta - \mu) I(m_{\tilde{t}_1}, m_{\tilde{t}_2}, \mu). \quad (12)$$

One finds that over the parameter space scanned, the NLO effects arising from the SQCD corrections of the top Yukawa coupling (gluino-squark loop diagrams) that in turn affect the contributions from the $t-H^{\pm}$ loops may have significant role in $\mathrm{BR}(b\to s\gamma)$. Typically, these NLO corrections are known to be important for large values of $\tan\beta$. But in spite of $\tan\beta$ being small in our analysis, the same corrections are also very important because of possible large values of μ [51] considered in this work. The reason is that these NLO corrections are approximately proportional to $\mu M_{\tilde{g}} \tan\beta$ [50,51]. Thus, regions of parameter space with large values of μ may change the $\bar{t}bH^+$ coupling leading to a reduction of $t-H^{\pm}$ loop contributions to $\mathrm{BR}(b\to s\gamma)$ [50]. Furthermore, as seen in Eq. (12), the SQCD corrections to Δm_b can be substantially large in spite of the fact that $\tan\beta$ is small in our analysis. This will have an overall suppression effect of the aforesaid SUSY loop contributions to $\mathrm{BR}(b\to s\gamma)$ over the valid parameter space of interest with large and positive values of μ and A_t. We note that the valid regions of parameter space that satisfy $\mathrm{BR}(b\to s\gamma)$ correspond to heavy enough SUSY spectra and do not involve cancellation between the two basic types of SUSY loop diagrams. We have further imposed the constraint from $\mathrm{BR}(B_s\to\mu^+\mu^-)$ [56,57] in this analysis. In the parameter space that survives after imposing the constraint from $\mathrm{BR}(b\to s\gamma)$ it turns out that $\mathrm{BR}(B_s\to\mu^+\mu^-)$ does not take away any significant amount of parameter space because of its smaller SUSY contributions. This arises out of the cancellation of relevant terms for the positive sign of μA_t that gives rise to a positive value for the dimensionless Wilson coefficient of the semileptonic pseudoscalar operator (see Ref. [54] and references therein).

B. Benchmark points

We show Tables II–IV for the choice of two benchmark points (BP1 and BP2) allowed by the constraints from Eqs. (1) to (7). Apart from the above constraints, large values of μ and A_t in the valid region of parameter space

[4]SUSY electroweak corrections to the bottom Yukawa couplings can also be large for large μ [51].

TABLE II. Input parameters for the two benchmark points allowed by the constraints, Eqs. (1)–(7).

Point	BP1	BP2
	Input parameters	
$\tan\beta$	4.28	5.22
μ (GeV)	9333	9177
M_1 (GeV)	731.2	600.4
M_2 (GeV)	493.3	933.4
M_3 (GeV)	2056.7	3298
A_t (GeV)	7047.2	6994.9
A_b (GeV)	−4838.3	−2560.4
$M_{\tilde{Q}_{3L}}$ (GeV)	1473.7	1522.8
$M_{\tilde{t}_R}$ (GeV)	2806.9	3132.4
$M_{\tilde{b}_R}$ (GeV)	671.6	536.4
m_t (GeV)	173.1	174.3

TABLE III. Mass spectrum for the two benchmark points.

Point	BP1	BP2
	Mass spectrum	
M_h (GeV)	97.8	96.4
M_H (GeV)	126.5	127.9
$M_{H^{\pm}}$ (GeV)	191.8	175.02
M_A (GeV)	185.7	166.3
$m_{\tilde{g}}$ (GeV)	2230.6	3355.8
$m_{\tilde{t}_1}$ (GeV)	689.5	913.7
$m_{\tilde{t}_2}$ (GeV)	1409.2	2232.4
$m_{\tilde{b}_1}$ (GeV)	793.4	614.5
$m_{\tilde{b}_2}$ (GeV)	1560.9	1596.5
$m_{\tilde{\chi}_1^{\pm}}$ (GeV)	492.9	933.0
$m_{\tilde{\chi}_1^0}$ (GeV)	492.9	600.4
$m_{\tilde{\chi}_2^0}$ (GeV)	731.1	933.0

TABLE IV. A few relevant observables for the two benchmark points considered in Table II.

Point	BP1	BP2
	Values of the Observables	
$\mathrm{BR}(b\to s\gamma)\times 10^4$	3.65	3.85
$\mathrm{BR}(B_s\to\mu^+\mu^-)\times 10^9$	2.67	2.21
$\Omega_{\tilde{\chi}_1} h^2$	0.006	0.05
$\mu_{gg}^H(\gamma\gamma)$	1.00	1.35
$\sigma_{\tilde{\chi}p}^{\mathrm{SI}}\times 10^{10}$ (pb)	1.27	0.07
$\mu_{gg}^H(ZZ)$	0.93	1.31
$\mu_{gg}^H(W^+W^-)$	0.89	1.25
$\mu_{Vh/H}^H(b\bar{b})$	0.57	0.49
$\mu_{Vh/H}^H(\tau^+\tau^-)$	1.23	1.38

specially motivate us in analyzing the effect of imposing the CCB constraints in a general setup going beyond the traditional constraints of CCB (see Ref. [45] and references therein for details) as used in the code SuSpect. We particularly analyze the above for only these two BPs rather than the entire parameter space simply for economy of computer time. We analyze the BPs by considering nonvanishing vevs for the Higgs scalars and top-squarks. BP1 corresponds to a stable vacuum. BP2 has a cosmologically long-lived vacuum while allowing quantum tunneling. Moreover, the BPs are so chosen that the squark masses of the third generation lie above ∼600 GeV, sufficiently large to be safely above the current bounds from the LHC. For BP1 $m_{\tilde{\chi}_1^\pm} \simeq m_{\tilde{\chi}_1^0}$ and $\tilde{\chi}_1^0$, which is the lightest SUSY particle (LSP) in our case, is almost winolike. Thus, the mechanisms which lead to right relic density of the DM are mainly $\tilde{\chi}_1^0 - \tilde{\chi}_1^\pm$ coannihilation and $\tilde{\chi}_1^\pm$ mediated $\tilde{\chi}_1^0$ pair annihilation to $W^\pm$. The strong annihilation and coannihilations make the LSP under-abundant. $m_{\tilde{\chi}_1^\pm}$ is taken to be above 270 GeV so as to be consistent with the results from the disappearing charged tracks searches at the LHC (which impose a lower limit of 270 GeV for the masses of the winolike LSPs [58]). The LSP in BP2 is predominantly a bino. The main annihilation mechanism in this case is the annihilation of sbottom pairs into a pair of gluons in the final state. The spin-independent $\tilde{\chi}_1^0$-proton scattering cross section $\sigma^{\rm SI}_{\tilde{\chi}p}$ is also seen to be well below the limit provided by the LUX experiment in both the cases. The smallness of $\sigma^{\rm SI}_{\tilde{\chi}p}$ arises as a result of large values of μ considered in this study leading to a negligible Higgsino component within the LSP [59].

IV. PROSPECTS AT THE HIGH-LUMINOSITY RUN OF THE LHC

In the last section we studied the available parameter space in the MSSM consistent with the ILLH scenario and also provided two benchmark points allowed by the LHC as well as low energy physics data. In this section, we proceed to discuss the sensitivity of the high-luminosity run of the LHC to probe the ILLH scenario. We start with the possibility to discover/exclude a 98 GeV Higgs boson produced through the VBF and Higgs-strahlung processes. Note that, the reason behind our choice of the two above-mentioned processes is that the Higgs boson production cross section is directly proportional to the Higgs to gauge boson coupling, $\sin^2(\beta-\alpha)$. Moreover, to satisfy the LEP excess we require $\sin^2(\beta-\alpha) \sim 0.2$. Thus, if we observe a Higgs boson with mass ∼100 GeV in the associated/VBF processes with cross sections ∼20% of the SM cross section, that can be thought of as a smoking gun signal of the ILLH scenario. Furthermore, we also analyze how the future precision measurements of various Higgs signal strength variables may be used as an indirect probe for the ILLH scenario.

A. Direct search: 1. Vector boson fusion process

The VBF process, $pp \to jjH$, (where j stands for light jets) is one of the most promising channels for the measurement of various properties of the observed 125 GeV Higgs boson at the LHC. It is a t-channel scattering process of two initial-state quarks with each one radiating a W/Z which further annihilates to produce a Higgs boson. Characteristic features of this process are the presence of two energetic jets with a large rapidity gap along with a large invariant mass and the absence of a significant amount of hadronic activity in the central rapidity region. Even though the ggF process is the dominant production mechanism for the Higgs boson, due to the above distinctive features, VBF is sensitive enough to a precise measurement of various properties of the observed Higgs boson.

The ATLAS Collaboration estimated the sensitivity of the VBF process for low mass Higgs bosons ($M_H < 130$ GeV), where the $H \to \tau^+\tau^-$ decay mode was considered at the 14 TeV LHC [60]. In the present work we perform a collider analysis following the ATLAS simulation to probe the discovery potential of the 98 GeV Higgs boson at the LHC-14. The ATLAS simulation considered three different decay modes of τ, namely, $\tau_\ell\tau_\ell$, $\tau_\ell\tau_h$, $\tau_h\tau_h$ where τ_ℓ and τ_h denote the leptonically and hadronically decaying τ-leptons respectively. From their analysis it is evident that the $\tau_\ell\tau_h$ channel has the best sensitivity compared to the other two possible modes (see Fig. 16 of Ref. [60]). Thus, in this work we confine ourselves in the $\tau_\ell\tau_h$ channel only. Note that, even though we follow the ATLAS simulation for our analysis, we further vary the selection cuts to optimize the signal to background ratio.

In order to tag the τ-leptons as τ-jets, we first identify τ through its hadronic decays and then demand that the candidate jet must have $|\eta| < 2.5$ and $p_T > 30$ GeV. Besides, the jet must also contain one or three charged tracks with $|\eta_{\rm track}| < 2.5$ with the highest track $p_T > 3$ GeV. To ensure proper charged track isolation, we additionally demand that there are no other charged tracks with $p_T > 1$ GeV within the candidate jet. The ditau invariant mass is calculated using the "collinear approximation technique" assuming the τ-lepton and its decay products to be collinear [61] and the neutrinos to be the only source[5] of $\not{E}_T$. Neglecting the τ rest mass, the ditau invariant mass can be written as

$$m^2_{\tau\tau} = 2(E_h + E_{\nu h})(E_\ell + E_{\nu\ell})(1 - \cos\theta_{\ell h}), \qquad (13)$$

where E_h and E_ℓ represent the total energy of the hadronically and leptonically decaying τ's, respectively, while $\theta_{\ell h}$

[5]An alternative technique preferred by the experimental collaborations is the missing mass calculator method for the reconstruction of $\tau\tau$ invariant mass [61]. In this paper, however, we restrict ourselves to the "collinear approximation technique".

represents the azimuthal angle between the directions associated with the above two decay modes of the τ-lepton. We can now introduce two dimensionless variables x_ℓ and x_h, the fraction of τ's momentum taken away by the visible decay products, and rewrite the di-tau invariant mass as follows (with $x_{\ell,h} > 0$):

$$m_{\tau\tau} = \frac{m_{\ell h}}{\sqrt{x_\ell x_h}}, \tag{14}$$

where $m_{\ell h}$ is the invariant mass of the visible τ-decay products, and

$$x_h = \frac{E_h}{(E_h + E_{\nu h})}, \qquad x_l = \frac{E_l}{(E_l + E_{\nu l})}. \tag{15}$$

Our event selection prescription involves four independent parameters which we vary in order to optimize the signal significances. These are the minimum transverse momentum p_T of the hadronic τ-lepton ($p_T^{\tau_h}$), minimum missing transverse energy ($\not{E}_T^{\rm min}$), minimum transverse momentum of the two leading jets ($P_{T,j}^{\rm min}$), and minimum of the di-jet invariant mass ($m_{j_1 j_2}^{\rm min}$). We proceed in the following steps.

(i) C1: We demand the presence of exactly one lepton (electron or muon) with $p_T^e > 25$ GeV or $p_T^\mu > 20$ GeV.
(ii) C2: We identify hadronic τ with $p_T > p_T^{\tau_h}$ and charge opposite to that of the identified lepton.
(iii) C3: We select events with missing transverse energy $\not{E}_T$ greater than $\not{E}_T^{\rm min}$.
(iv) C4: The variables associated to di-tau invariant mass reconstruction satisfy $0 \le x_l \le 0.75$, $0 \le x_h \le 1$, and $\cos\Phi_{lh} \ge -0.9$.
(v) C5: A cut on the transverse mass(m_T) of the lepton and $\not{E}_T$ is applied to suppress the $W+$jets and $t\bar{t}$ backgrounds, where

$$m_T^2 = 2p_T^l \not{E}_T (1 - \cos\Delta\Phi), \tag{16}$$

with $p_T^{\rm lep}$ representing the transverse momentum of the lepton and $\Delta\Phi$ is the angle between that lepton and $\not{E}_T$ in the transverse plane. We demand $m_T < 30$ GeV.
(vi) C6: We require the leading two jets to satisfy $p_T \ge p_{T,j}^{\rm min}$.
(vii) C7: The forward jets should lie in opposite hemispheres $\eta_{j_1} \times \eta_{j_2} \le 0$ with tau centrality $\min(\eta_{j_1}, \eta_{j_2}) \le \eta_{{\rm lep},\tau} \le \max(\eta_{j_1}, \eta_{j_2})$ for the two highest p_T jets.
(viii) C8: Forward jets should also satisfy $\Delta\eta_{j_1 j_2} \ge 4.4$ and di-jet invariant mass $m_{j_1 j_2} \ge m_{j_1 j_2}^{\rm min}$.
(ix) C9: The events are rejected if there are any additional jets with $p_T \ge 20$ GeV with $|\eta| \le 3.2$.
(x) C10: Finally, we select the events with di-tau invariant mass satisfying $90\,{\rm GeV} \le m_{\tau\tau} \le 110\,{\rm GeV}$.

TABLE V. Details of the different signal regions are given. The kinematic selection cuts obtained from the ATLAS simulation is denoted by SR0, while our optimized selection cuts are described by SRA and SRB. For details see the text.

Signal Regions	$p_T^{\tau_h}$	$\not{E}_T^{\rm min}$	$p_{T,j}^{\rm min}$	$m_{j_1 j_2}^{\rm min}$
SR0	20.0	30.0	20.0	700.0
SRA	80.0	80.0	60.0	1200.0
SRB	50.0	50.0	40.0	1500.0

TABLE VI. Expected number of events at the 14 TeV LHC with 3000 fb^{-1} of integrated luminosity within a mass window of 90–110 GeV for individual signal and total background. We assume that the signal cross section is 20% of the SM value calculated with the Higgs mass $m_h^{\rm SM} = 98$ GeV. The signal significances are calculated using systematic uncertainty $\kappa = 0.2$.

	SR0	SRA	SRB
Signal (S)	271.3	25.4	71.0
Backgrounds (B)	1713.3	55.3	221.1
Significance $\left(\mathcal{S} = \frac{S}{\sqrt{B+\kappa^2 B^2}}\right)$	0.78	1.91	1.52

The possible SM backgrounds in this case come from $t\bar{t}+$jets, $W+$jets, $Z+$jets, and di-boson final states (WW, ZZ, WZ). From the ATLAS simulation [60], we find that $Z+$jets is the most dominant background with $Z \to \tau^+\tau^-$. Hence, in our analysis, we simulate only the $Z+$jets background. We use MADGRAPH5 (v1 2.2.2) [62] to generate the background events and then hadronize the events using PYTHIA (version 6.4.28) [63]. Table V shows the optimized set of cuts. The expected number of signal and background events at the 14 TeV run of the LHC with 3000 fb^{-1} of integrated luminosity within a mass window of 90–110 GeV and the resulting statistical significances for three optimized scenarios are presented in Table VI. We obtain a maximum of 1.9σ significance for the signal region SRA with 3000 fb^{-1} of data. Note that we have considered only the dominant background $Z+$jets. However, we expect the significances to be reduced even further if we consider all the possible backgrounds. Thus, we conclude that the possibility of observing the 98 GeV Higgs boson via VBF process at the 14 TeV LHC run is rather poor even at an integrated luminosity of 3000 fb^{-1}.

B. Direct search: 2. Associated production

Another important production mode of the 98 GeV Higgs boson is the Higgs-strahlung process where the Higgs is produced in association with a gauge boson W/Z. In our earlier work [9], we discussed the discovery potential of the 98 GeV Higgs boson produced via this process giving special attention to the boosted regime with the

TABLE VII. Different signal regions for the three processes considered in this analysis. The default ATLAS simulation is denoted by SR0, while our optimized selection cuts are described by SRA, SRB, and SRC for the three processes.

Process	Signal Regions	Selection Cuts				
		$p_{T,Z}^{\min}$	$p_{T,j_1}^{\min}$	$\Delta\Phi_1$	$p_T^{\ell_1}$	$p_T^{\ell_2}$
3-7 $\ell^+\ell^- b\bar{b}$	SR0	180	200	1.2	25	20
	SRA	250	250	1.2	100	50
		$p_{T,W}^{\min}$	$p_{T,j_1}^{\min}$	$\Delta\Phi_1$	$\not{p}_T^{\min}$	
$\ell^+\nu_\ell b\bar{b}$	SR0	180	200	1.2	30	
	SRB	300	300	1.5	75	
		$p_{T,j_1}^{\min}$	$\Delta\Phi_1$	$\not{p}_T^{\min}$		
$\not{E}_T b\bar{b}$	SR0	200	1.2	200		
	SRC	250	1.5	300		

assumption that it was produced with $p_T > 200$ GeV. It is pertinent to note that in Ref. [9] we took the number of background events directly from the ATLAS simulation [64]. However, in this work, we perform a more detailed Monte Carlo simulation by generating both the signal and background events and then optimizing the event selection cuts. We again focus on the boosted regime here. Note that even though the production cross section is very small in this highly boosted regime (p_T of the Higgs is greater than 200 GeV), relatively large kinematic acceptance and large background reduction make this analysis special. The details of our collider analysis can be found in Ref. [9]. However, we give a very brief outline of our analysis below. We divide this part of our analysis into three categories based on the decay modes of the gauge bosons, namely,

(1) Wh process with W decaying leptonically with missing transverse momentum $\not{p}_T > \not{p}_T^{\min}$ and $p_T^{e/\mu} > 30$ GeV. The transverse momentum of the W-boson must also satisfy $p_T > p_{T,W}^{\min}$. Here we vary the quantities $\not{p}_T^{\min}$ and $p_{T,W}^{\min}$ independently.

(2) Zh process with Z decaying into a pair of leptons (e/μ) with di-lepton invariant mass satisfying 80 GeV $< m_{\ell\ell} <$ 100 GeV while p_T^Z exceeds certain minimum value $p_{T,Z}^{\min}$. We also vary the transverse momentum of the two leptons independently.

(3) Finally, missing transverse energy driven signal with no leptons and $\not{E}_T > \not{E}_T^{\min}$. This kind of signature mainly comes from the process Zh when Z-boson decays invisibly to a pair of neutrinos. However, contributions from Wh process may also come when the lepton from W remains undetected.

In the above, $p_T^{\min}$ refers to the minimum p_T of the Higgs required to claim the jet to be a *Fat jet* with $|\eta| < 2.5$. Similar to our VBF analysis, we first analyze the ATLAS optimized cuts and then vary some of the important observables relevant to a specific process so as to obtain the maximum sensitivity of the given channel. For example, for the $\ell^+\ell^- b\bar{b}$ channel we vary the transverse momentum of the Higgs jet, Z-boson, and the pair of leptons to get the maximum signal significance. A similar strategy has been opted for other modes. The default selection cuts for a given channel have been denoted as "SR0," while our optimized selection cuts are represented as "SRA," "SRB," and "SRC" for the $\ell^+\ell^- b\bar{b}$, $\ell^+\nu_\ell b\bar{b}$, and $\not{E}_T b\bar{b}$ signals, respectively (see Table VII). We use PYTHIA (version 6.4.28)[63] for generation of signal events while FASTJET (version 3.0.3)[65] is used for the reconstruction of jets and also implementation of the jet substructure analysis. The most dominant SM backgrounds for our process of interest are WW, ZZ, WZ, $Wb\bar{b}$, $Zb\bar{b}$, and $t\bar{t}$. We use MADGRAPH to generate the $Wb\bar{b}$, $Zb\bar{b}$ samples and then passed them to PYTHIA for showering and hadronization while the rest of the background samples are generated using PYTHIA itself.

TABLE VIII. Expected number of events at the 14 TeV LHC run with 3000 fb^{-1} of integrated luminosity within a mass window of 90–110 GeV for the individual signal and the combined background processes assuming 20% LEP excess in this region of interest.

Process	Signal Region	Signal (S)	Background (B)	Significance $\left(\frac{S}{\sqrt{B+\kappa^2 B^2}}\right)$
$\ell^+\ell^- b\bar{b}$	SR0	184.9	956.1	0.95
	SRA	94.8	168.7	2.62
$\ell\nu b\bar{b}$	SR0	360.2	1998.4	0.89
	SRB	99.5	185.8	2.51
$E\!\!\!/_T b\bar{b}$	SR0	184.9	2614.3	0.35
	SRC	94.8	297.2	1.53

We present our final results in Table VIII where we scale the cross sections by 0.2 and focus in the mass window 90–110 GeV to satisfy the 2.3σ LEP excess. In Table VIII we display the expected number of events for the signal and various backgrounds with 3000 fb^{-1} of luminosity. The statistical significances for the signal regions SR0 (the default ATLAS parameters) as well as SRA, SRB, and SRC (our optimized sets) are also shown for the three possible decay modes. We find that the best sensitivity comes from the channel $\ell^+\ell^- b\bar{b}$ with 2.6σ significance, while $\ell^+\nu_\ell b\bar{b}$ and $E\!\!\!/_T b\bar{b}$ have statistical significances of 2.5σ and 1.5σ, respectively. We must note that although we assume 20% systematic uncertainty (i.e., $\kappa = 0.2$), nevertheless with 3000 fb^{-1} of luminosity we can expect to have a better control over the various sources of systematic uncertainties leading to an enhanced signal significance. Therefore, one can expect to marginally exclude the 98–125 GeV Higgs scenario using 3000 fb^{-1} of data at the 14 TeV LHC via the Higgs-strahlung process.

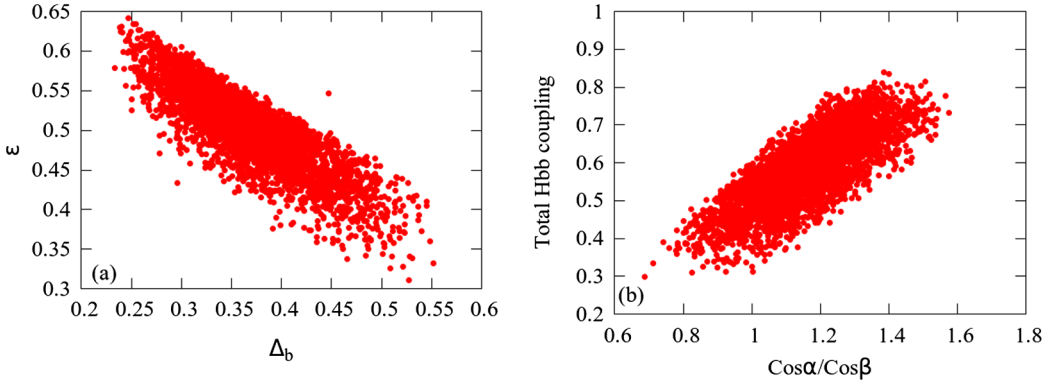

FIG. 4. Left panel shows the distribution of the quantity $\epsilon = (\frac{1}{1+\Delta_b}) \times (1 + \Delta_b \cot\beta \tan\alpha)$ with the variation of Δ_b. The variation of the total Yukawa coupling of the bottom quark with the heavier Higgs boson with respect to the tree level coupling $\frac{\cos\alpha}{\cos\beta}$ is shown in the right panel.

C. Indirect search: Higgs coupling measurements

Precise measurement of the various Higgs signal strength variables can prove to be significant to indirectly probe/exclude the ILLH scenario. We find that the important observables which can play crucial roles in this regard are μ_{bb}, $\mu_{\tau\tau}$, and μ_{ZZ} for a given production mechanism of the observed 125 GeV Higgs boson. Before going into a detailed analysis of these observables, let us first discuss some of the important Higgs boson couplings. The tree level Yukawa coupling of the bottom quark with the heavy Higgs boson of the MSSM having a mass around 125 GeV goes as $\frac{\cos\alpha}{\cos\beta}$ where $\tan\beta$ is the ratio of the vevs of the two Higgs doublets. However, loop corrections (in orders of $\alpha_s \tan\beta$) involving various supersymmetric particles can significantly modify the tree level $Hb\bar{b}$ Yukawa coupling. These effects are generally denoted by the quantity Δ_b and the additional contribution coming from Δ_b can be summarized as [51,66–68]

$$\epsilon = \left(\frac{1}{1+\Delta_b}\right) \times \left(1 + \Delta_b \cot\beta \tan\alpha\right). \qquad (17)$$

In the left panel of Fig. 4, we show the dependence on Δ_b of the quantity ϵ which estimates the loop contribution to the tree level Yukawa coupling. We find that the effect of Δ_b is indeed significant in the parameter space of our interest. In the right panel of Fig. 4, we show the variation of the complete $Hb\bar{b}$ coupling (the effect of Δ_b included) with the tree level coupling. It is evident from both the figures that for a significant number of points Δ_b is indeed large. Thus, even though the maximum value of the tree level coupling goes up to 1.4–1.5, the total $Hb\bar{b}$ coupling never exceeds unity, implying that the $Hb\bar{b}$ coupling is always suppressed with respect to the SM expectation which can indeed serve as a very distinctive feature of the ILLH scenario.

Let us now turn our attention to another important decay mode $H \to ZZ^*$. In the left panel of Fig. 5, we show the variation of the ratio $\Gamma_{ZZ}/\Gamma_{ZZ}^{\rm SM}$ to the square of the tree level HZZ coupling $\sin(\beta-\alpha)$. Here, Γ_{ZZ} denotes the partial width of the decay $H \to ZZ^*$ in the MSSM and $\Gamma_{ZZ}^{\rm SM}$ denotes the same for the SM. The behavior is well understood; as the coupling decreases so does the partial width. However, we must note that the $H \to ZZ^*$ partial width is also suppressed in this case. With both the partial widths for

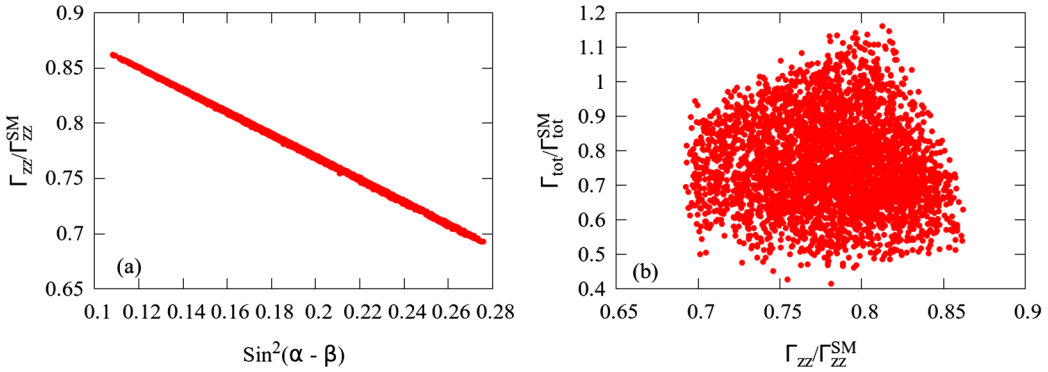

FIG. 5. The correlation of the partial decay width of Higgs to ZZ^* decay with $\sin^2(\beta-\alpha)$ (left panel) and with total Higgs decay width $\Gamma_{\rm tot}$ (right panel).

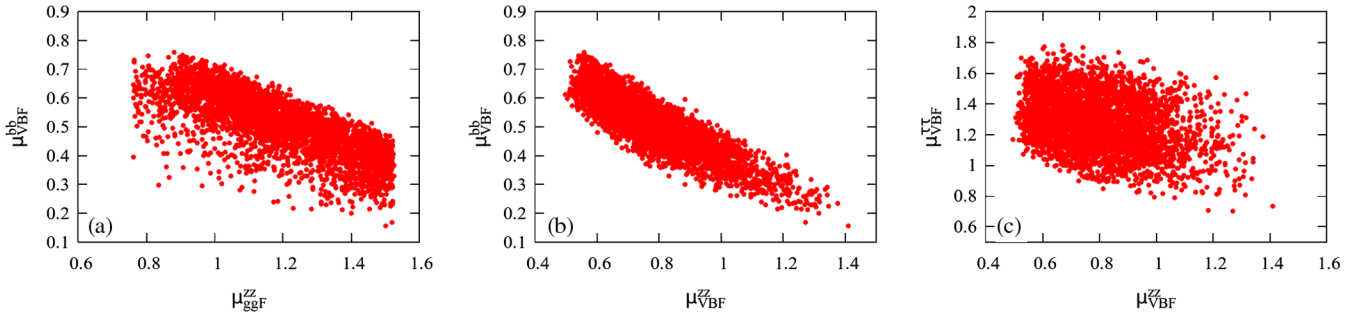

FIG. 6. Correlation plots in μ^{ZZ}_{ggF}-μ^{bb}_{VBF} (left), μ^{ZZ}_{VBF}-μ^{bb}_{VBF} (middle), and μ^{ZZ}_{VBF}-$\mu^{\tau\tau}_{VBF}$ (right) planes. For details see the text.

the decays $H \to b\bar{b}$ and $H \to ZZ^*$ suppressed, one can expect to observe a significant suppression in the total decay width of the Higgs boson as well. From the plot in the right panel of Fig. 5, where the x axis denotes the ratio $\Gamma_{ZZ}/\Gamma^{\rm SM}_{ZZ}$ and the y axis stands for the ratio of the total Higgs decay width ($\Gamma_{\rm tot}$) in the MSSM to that in the SM ($\Gamma^{\rm SM}_{\rm tot}$), one can easily observe the suppression in the total decay width. Thus, one may also expect to find a mild enhancement in partial widths of the subdominant decay modes like $\tau^+\tau^-$, gg.

Improved measurement of the signal strength variables at the high-luminosity run of the LHC may help us to probe the ILLH scenario indirectly. We present a detailed study in this regard as follows. We have already introduced the signal strength variables in Sec. II. Here, we discuss the variables which we find interesting and which are seen to have some impact to probe/exclude the parameter space of our interest. In the leftmost panel of Fig. 6, we display the correlation in the μ^{ZZ}_{ggF}-μ^{bb}_{VBF} plane. We assume the ggF process as the production mechanism for the Higgs boson decaying into ZZ while for the final state $b\bar{b}$ the Higgs is taken to be produced via the VBF process. We find that although μ^{ZZ}_{ggF} can vary in the range 0.6–1.6, the values of μ^{bb}_{VBF} are seen to be suppressed, i.e., less than unity. Furthermore, even though the gluon-gluon fusion process is the dominant one, associated production mechanism of the Higgs can also be used to measure these signal strength variables. We discuss the correlations of three such variables, namely μ^{ZZ}_{VBF}, μ^{bb}_{VBF}, and $\mu^{\tau\tau}_{VBF}$. In the middle and rightmost panel we show the correlations in the μ^{ZZ}_{VBF}-μ^{bb}_{VBF} and μ^{ZZ}_{VBF}-$\mu^{\tau\tau}_{VBF}$ planes, respectively. Similar to the ggF case, there are no such restrictions on the values of μ^{ZZ}_{VBF}. However, we find a strong anticorrelation between μ^{bb}_{VBF} and $\mu^{\tau\tau}_{VBF}$. The values of μ^{bb}_{VBF} are found to be always less than unity while those of $\mu^{\tau\tau}_{VBF}$ are found to be dominantly greater than unity. At this point, one might be interested to know the present status of the measurement of these Higgs signal strength correlations at the LHC. In Fig. 7, we study these correlations in the $\mu^{f}_{ggF+t\bar{t}H}$-μ^{f}_{VBF+VH} plane for a generic final state f, and then compare the model predictions with the 95% correlation contours obtained using the 10-parameter fit for the five decay modes of the observed Higgs boson by the ATLAS and CMS combined 7 and 8 TeV data [31]. In the left panel, we show $\gamma\gamma$, ZZ, and WW channels while in the right panel we show the $b\bar{b}$ and $\tau^+\tau^-$ channels. The subscript F denotes the combined ggF and $t\bar{t}H$ processes, while V signifies the combined VBF and VH processes. However, here for the fusion

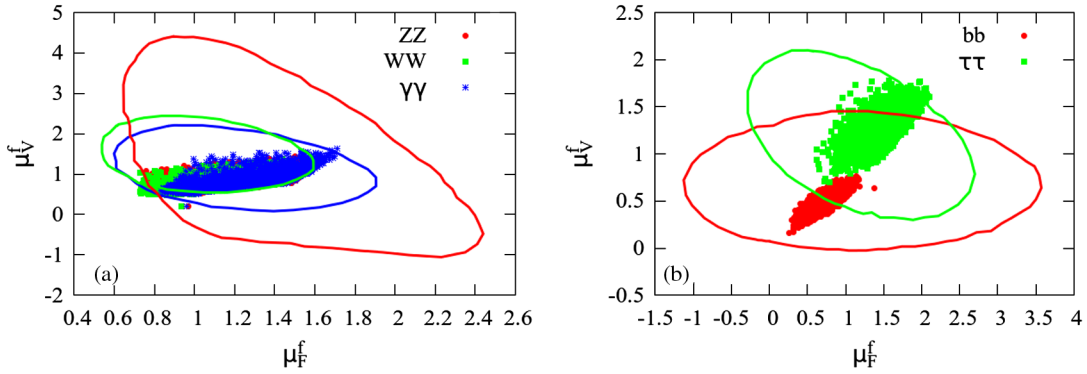

FIG. 7. The 95% C.L. contours in the $\mu^{f}_{ggF+t\bar{t}H}$-μ^{f}_{VBF+VH} plane with the ATLAS and CMS combined 7 and 8 TeV data for five possible decay modes: in the left we show $\gamma\gamma$, ZZ, and WW channels while in the right panel we show $b\bar{b}$ and $\tau^+\tau^-$. The subscript F denotes the combined ggF and $t\bar{t}H$ process, while V signifies the combined VBF and VH processes. However, here for the fusion (F) mode we consider ggF only, as Higgs production via ggF is much larger compared to the $t\bar{t}H$ process. See the text for more details.

(F) mode we consider ggF only as Higgs production via ggF is much larger compared to the $t\bar{t}H$ process. Comparing the correlation plots (Fig. 7) with Table I, we find that at present the impact of these correlations at the parameter space of interest is comparable with that of the individual signal strengths (less than 2% points are found to be outside the 95% C.L. contours). However, here we would like to note that with precise measurements in the future runs of LHC these contours are expected to shrink, which may lead to interesting consequences for our model parameter space. Considering the future improvements in signal strength measurements, if we assume that at the high-luminosity run of the LHC with 3000 fb^{-1} of data μ_{VBF}^{ZZ} can be measured with an accuracy at the level of 30%, then from these correlations we can infer that $\mu_{VBF}^{\tau\tau}$ will always have values larger than unity. However, μ_{VBF}^{bb} will be less than 0.8. Thus, for a given measurement of the signal strength variable in the ZZ channel, observation of suppression of the same quantity for the $b\bar{b}$ channel and enhancement in the $\tau\tau$ channel will be an ideal probe of the ILLH scenario.

Before we end this section, let us summarize our results from the collider analysis. We analyze the most important production mechanism of the 98 GeV Higgs boson, namely the VBF and associated production processes, and find that these processes are not sensitive enough to exclude the ILLH scenario. We then attempt to exclude this possibility indirectly using various Higgs signal strength variables, and here we find very distinctive features in the correlations of the signal strength variables for bb, $\tau\tau$, and ZZ decay channels. However, there exists several other processes which can also be used directly to probe this scenario, e.g., the associated production of the 98 GeV Higgs boson with a pair of top quarks ($t\bar{t}h$). Even though this process does not directly involve the $\sin^2(\beta-\alpha)$ coupling, still it can be used to probe this scenario. In our earlier work [9], we performed a naive collider analysis of this process, following the same analysis for a SM Higgs boson [69], and obtained a 2.6σ statistical significance without considering systematic uncertainties. A more detailed study is required, specially focusing on the boosted regime and applying the jet substructure technique, which is beyond the scope of the present work. Interestingly, we can also discover/exclude the 98–125 GeV Higgs scenario by looking for the other Higgses present in this model, e.g., the neutral CP-odd Higgs A and the charged Higgs bosons $H^{\pm}$. One of the most important characteristic signatures of this ILLH scenario is the presence of relatively light A and $H^{\pm}$ bosons with masses $\lesssim$200 GeV. The pseudoscalar Higgs A is produced via gluon-gluon fusion and/or $b\bar{b}$ fusion processes and, if kinematically allowed, can decay to Zh giving rise to interesting final state topologies involving multileptons and multiple b-jets. On the other hand, the charged Higgs bosons are produced by $tbH^{\pm}$ process and decay dominantly into $\tau\nu_{\tau}$ and $t\bar{b}$ final states. A dedicated analysis for these very light CP-odd and charged Higgses in the context of the high-luminosity run of the LHC is required. We leave this very interesting possibility for our future work. Thus, the observation of a charged Higgs and a pseudoscalar Higgs boson with masses between 140–200 GeV and simultaneously the nonobservation of any CP-even Higgs in the same region will be a direct probe of the ILLH scenario. Furthermore, productions of these light Higgses in pair, e.g., processes like $H^{\pm}A$, $H^{+}H^{-}$, $H^{\pm}h$, Ah are also very interesting possibilities at the LHC. There exists a study considering all of these processes at the LHC in the context of the nondecoupling region of the MSSM [13]. However, the authors focused only on the regions with masses of these Higgses lying between 95–130 GeV. Note that, this 95–130 GeV region is already excluded by the pseudoscalar and charged Higgs searches at the LHC, and thus a study focussing on the region 140–200 GeV is now required, which we plan to address in our future correspondence. We would like to mention that in our earlier work we discussed the possibility of observing the 98 GeV Higgs boson directly at the ILC. We found that the above could be easily discovered/excluded at the 250 GeV ILC with a 100 fb^{-1} of luminosity which is easily achievable within the first few years of its run. Finally, we would like to add one important point regarding the direct measurement of various SUSY particles at the HL run of LHC. The expected exclusion limits at the HL-LHC for the top and bottom squarks are around 1 TeV, for charginos and neutralinos around 600 GeV while for gluinos they are around 2.5 TeV [70]. We check that even with such a heavy sparticle spectrum, there is ample parameter space which satisfies the current LHC data; thus, we conclude that it is almost impossible to exclude the 98–125 GeV scenario even at the high-luminosity run of LHC.

V. SUMMARY AND CONCLUSIONS

The objective of this work is to interpret the LEP excess observed around a mass of ∼98 GeV as the lighter CP-even Higgs boson of the MSSM while the LHC-observed scalar at ∼125 GeV plays the role of the heavier one. We analyze this scenario in the light of the latest results from the LHC including the limits on Higgs signal strengths. Other relevant constraints like those coming from the flavor sector, e.g., $\text{BR}(b\to s\gamma)$, $\text{BR}(B_s\to\mu^+\mu^-)$, and the DM relic density constraint are also taken into account. The ATLAS/CMS searches in the $H/A\to\tau^+\tau^-$ and charged Higgs searches restrict the values of $\tan\beta$ to a very narrow range. By performing a detailed random scan over the MSSM parameter space we try to pinpoint the region of parameter space where all the above constraints can be simultaneously accommodated. We observe that the ILLH scenario can still be harbored within the MSSM framework. The values of μ required to satisfy the above criteria are

generically large $\gtrsim 7$ TeV and A_t tends to assume only appreciably large positive values.

To perform the analysis in a model-independent way we use the limits on $\sigma \times \mathrm{BR}(\Phi \to \tau^+\tau^-)$, σ being the production cross section of the nonstandard Higgs boson Φ. The LHC limits are available for ggF and VBF production processes. We observe that $\sigma(ggF) \times \mathrm{BR}(\Phi \to \tau^+\tau^-)$ lies well below the experimental limit for the small values of $\tan\beta$ considered in this analysis. However, the values of this observable for associated production with $b\bar{b}$ seems to be very close to the present experimental bound.

In the ILLH scenario that is associated with a light $H^\pm$, the constraint from $\mathrm{BR}(b \to s\gamma)$ plays an important role to eliminate a large region of parameter space. We remember that the associated SM contributions almost saturate the experimental limit. Generally, the $\tilde{\chi}_1{}^\pm - \tilde{t}_1$ loop contributions are not large enough to effectively cancel the contributions from the $H^\pm - t$ loops where $H^\pm$ is light. This causes a large amount of the parameter space to be discarded. It is only for a large μ zone (with large A_t values) along with $\mathrm{sign}(\mu A_t) > 0$ that the NLO contributions arising out of the top-quark Yukawa coupling partially cancel the leading order contributions of the $H^\pm - t$ loops. Additionally, there is an overall suppression coming out of SQCD corrections to the mass m_b. Thus, the available parameter space that satisfies the $\mathrm{BR}(b \to s\gamma)$ constraint has large values of μ with $\mathrm{sign}(\mu A_t) > 0$. The other constraint, namely, $\mathrm{BR}(B_s \to \mu^+\mu^-)$ is not a very stringent one in this zone of parameter space that survives the $\mathrm{BR}(b \to s\gamma)$ constraint.

An important result regarding the Higgs signal strength variables is obtained when we closely study the points satisfying all the constraints along with the limits on $R^H_{gg}(\gamma\gamma)$. If we further demand that values of $R^H_{gg}(ZZ)$ lie within 20% around the SM value of unity, all the points are seen to have $R^H_{VH}(bb) \lesssim 0.8$. As already mentioned, the loop correction to the bottom quark Yukawa coupling and hence to the bottom quark mass (Δm_b) is significantly large in the present case. This reduces the partial decay width $\Gamma_{(H\to b\bar{b})}$. The value of $\Gamma_{(H\to ZZ)}$ is also small, leading to a reduction in the total decay width. However, the $\mathrm{BR}(H \to ZZ)$ can be significantly large. Thus, for the points with $0.8 < R^H_{gg}(ZZ) < 1.2$ the value of $R^H_{VH}(bb)$ is seen to be $\lesssim 0.8$. This can play a major role as a distinctive feature of the present scenario provided the sensitivity on the coupling strength measurements is increased to a desired accuracy.

We analyze the possibilities of observing the ILLH scenario in the 14 TeV run of the LHC in two production channels, the vector boson fusion process and associated production with the W/Z-boson. For the VBF process we follow the ATLAS simulation for the decay mode $H \to \tau_l\tau_h$. The selection cuts are varied to obtain an optimum signal to background ratio. We simulate only the $Z +$ jets events as the dominant SM background in this analysis. From statistical significances of the three optimized scenarios considered here we conclude that the possibility of observing the ILLH scenario with 3000 fb^{-1} of luminosity is rather small.

For the Higgstrahlung processes we concentrate on the highly boosted regime where the Higgs boson of mass 98 GeV is produced with $p_T > 200$ GeV. Three different scenarios are considered here depending on the decays of the associated gauge boson. These are the WH process with W decaying leptonically, the ZH process with Z decaying to the e/μ pair, and the ZH process with invisible decays of the Z-boson. We generate both the signal and background events through a detailed Monte Carlo simulation following the ATLAS analysis. The results are presented for three optimized selection regions along with the one using default selection cuts. From the results we observe that the ILLH scenario can be marginally ruled out with 3000 fb^{-1} of luminosity at the 14 TeV run of the LHC.

Finally, we summarize our findings of the 98–125 GeV ILLH scenario as follows:

(i) The most updated LHC data along with the low energy physics flavor data and bounds from dark matter searches does not exclude the possibility of having a 98–125 GeV Higgs scenario. We provide two sample benchmark points in support of our results.

(ii) The possibility for direct detection of the 98 GeV Higgs boson at the run 2 of the LHC is marginal even after using the state-of-the-art jet substructure technique.

(iii) However, precise measurements of the Higgs signal strengths may act as an indirect probe of the ILLH scenario. We find interesting correlations between these signal strength variables. For example, the quantity $R_{b\bar{b}}$ is always less than unity, thus we find that if we can measure the Higgs signal strength associated to the Higgs decay to ZZ then we must see a strong suppression in the $b\bar{b}$ mode. We expect at the high-luminosity run of LHC these measurements will be improved by few orders of magnitude, and thus could easily be used as a probe of the ILLH scenario.

ACKNOWLEDGMENTS

The work of B. B. is supported by Department of Science and Technology, Government of INDIA under the Grant Agreement No. IFA13-PH-75 (INSPIRE Faculty Award). A. C. would like to thank the Department of Atomic Energy, Government of India for financial support. M. C. would like to thank the Council of Scientific and Industrial Research, Government of India for financial support. We gratefully acknowledge the help received from Abhishek Dey for running the code Vevacious for the benchmark points.

[1] G. Aad *et al.* (ATLAS Collaboration), Observation of a new particle in the search for the Standard Model Higgs boson with the ATLAS detector at the LHC, Phys. Lett. B **716**, 1 (2012); S. Chatrchyan *et al.* (CMS Collaboration), Observation of a new boson at a mass of 125 GeV with the CMS experiment at the LHC, Phys. Lett. B **716**, 30 (2012).

[2] M. Flechl (ATLAS for and CMS Collaborations), Higgs physics: Review of recent results and prospects from ATLAS and CMS, J. Phys. Conf. Ser. **631**, 012028 (2015).

[3] For reviews on supersymmetry, see, e.g., H. P. Nilles, Supersymmetry, supergravity and particle physics, Phys. Rep. **110**, 1 (1984); J. D. Lykken, Introduction to Supersymmetry, arXiv:hep-th/9612114; J. Wess and J. Bagger, *Supersymmetry and Supergravity*, 2nd ed. (Princeton University Press, Princeton, 1991).

[4] H. E. Haber and G. Kane, The search for supersymmetry: Probing physics beyond the standard model, Phys. Rep. **117**, 75 (1985); S. P. Martin, A Supersymmetry Primer, arXiv:hep-ph/9709356; D. J. H. Chung, L. Everett, G. Kane, S. King, J. Lykken, and L. Wang, The soft supersymmetry-breaking Lagrangian: theory and applications, Phys. Rep. **407**, 1 (2005).

[5] M. Drees, P. Roy, and R. M. Godbole, *Theory and Phenomenology of Sparticles* (World Scientific, Singapore, 2005); H. Baer and X. Tata, *Weak Scale Supersymmetry: From Superfields to Scattering Events* (Cambridge University Press, Cambridge, 2006).

[6] A. Djouadi, The anatomy of electroweak symmetry breaking Tome II: The Higgs bosons in the Minimal Supersymmetric Model, Phys. Rep. **459**, 1 (2008).

[7] R. Barate *et al.* (LEP Working Group for Higgs Boson Searches and ALEPH, DELPHI, L3, and OPAL Collaborations), Search for the standard model Higgs boson at LEP, Phys. Lett. B **565**, 61 (2003).

[8] S. Schael *et al.* (ALEPH, DELPHI, L3, OPAL, and LEP Working Group for Higgs Boson Searches Collaborations), Search for neutral MSSM Higgs bosons at LEP, Eur. Phys. J. C **47**, 547 (2006).

[9] B. Bhattacherjee, M. Chakraborti, A. Chakraborty, U. Chattopadhyay, D. Das, and D. K. Ghosh, Implications of the 98 GeV and 125 GeV Higgs scenarios in nondecoupling supersymmetry with updated ATLAS, CMS, and PLANCK data, Phys. Rev. D **88**, 035011 (2013).

[10] M. Drees, Supersymmetric explanation of the excess of Higgs-like events at CERN LEP Phys. Rev. D **71**, 115006 (2005).

[11] M. Drees, A Supersymmetric Explanation of the excess of Higgs-like events at the LHC and at LEP, Phys. Rev. D **86**, 115018 (2012).

[12] N. D. Christensen, T. Han, and S. Su, MSSM Higgs bosons at the LHC, Phys. Rev. D **85**, 115018 (2012); M. Asano, S. Matsumoto, M. Senami, and H. Sugiyama, Comprehensive analysis on the light Higgs boson scenario, Phys. Rev. D **86**, 015020 (2012); S. Scopel, N. Fornengo, and A. Bottino, Embedding the 125 GeV Higgs boson measured at the LHC in an effective MSSM: Possible implications for neutralino dark matter, Phys. Rev. D **88**, 023506 (2013).

[13] N. D. Christensen, T. Han, and T. Li, Pair production of MSSM Higgs bosons in the nondecoupling region at the LHC, Phys. Rev. D **86**, 074003 (2012).

[14] B. Bhattacherjee, A. Chakraborty, D. Kumar Ghosh, and S. Raychaudhuri, Using jet substructure at the LHC to search for the light Higgs bosons of the *CP*-violating MSSM, Phys. Rev. D **86**, 075012 (2012).

[15] R. Barbieri, D. Buttazzo, K. Kannike, F. Sala, and A. Tesi, One or more Higgs bosons?, Phys. Rev. D **88**, 055011 (2013).

[16] D. G. Cerdeo, P. Ghosh, C. B. Park, and M. Peir, Collider signatures of a light NMSSM pseudoscalar in neutralino decays in the light of LHC results, J. High Energy Phys. 02 (2014) 048.

[17] G. Belanger, U. Ellwanger, J. F. Gunion, Y. Jiang, S. Kraml, and J. H. Schwarz, Higgs Bosons at 98 and 125 GeV at LEP and the LHC, J. High Energy Phys. 01 (2013) 069.

[18] J. F. Gunion, Y. Jiang, and S. Kraml, Could two NMSSM Higgs bosons be present near 125 GeV?, Phys. Rev. D **86**, 071702 (2012).

[19] D. G. Cerdeno, P. Ghosh, and C. B. Park, Probing the two light Higgs scenario in the NMSSM with a low-mass pseudoscalar, J. High Energy Phys. 06 (2013) 031.

[20] N. E. Bomark, S. Moretti, S. Munir, and L. Roszkowski, A light NMSSM pseudoscalar Higgs boson at the LHC redux, J. High Energy Phys. 02 (2015) 044.

[21] N. E. Bomark, S. Moretti, and L. Roszkowski, Detection prospects of light NMSSM Higgs pseudoscalar via cascades of heavier scalars from vector boson fusion and Higgs-strahlung, arXiv:1503.04228.

[22] M. Badziak, M. Olechowski, and S. Pokorski, New Regions in the NMSSM with a 125 GeV Higgs, J. High Energy Phys. 06 (2013) 043.

[23] B. Allanach, M. Badziak, C. Hugonie, and R. Ziegler, Light sparticles from a light singlet in gauge mediation, Phys. Rev. D **92**, 015006 (2015).

[24] K. O. Astapov and S. V. Demidov, Sgoldstino-Higgs mixing in models with low-scale supersymmetry breaking, J. High Energy Phys. 01 (2015) 136.

[25] A. Arbey, J. Ellis, R. M. Godbole, and F. Mahmoudi, Exploring *CP* violation in the MSSM, Eur. Phys. J. C **75**, 85 (2015).

[26] G. Aad *et al.* (ATLAS Collaboration), Search for neutral Higgs bosons of the minimal supersymmetric standard model in pp collisions at $\sqrt{s} = 8$ TeV with the ATLAS detector, J. High Energy Phys. 11 (2014) 056 (2014).

[27] CMS Collaboration, Report No. CMS-PAS-HIG-14-029.

[28] ATLAS Collaboration, Report No. ATLAS-CONF-2013-090.

[29] CMS Collaboration, Report No. CMS-PAS-HIG-14-020.

[30] G. Degrassi, S. Heinemeyer, W. Hollik, P. Slavich, and G. Weiglein, Towards high precision predictions for the MSSM Higgs sector, Eur. Phys. J. C **28**, 133 (2003); B. C. Allanach, A. Djouadi, J. L. Kneur, W. Porod, and P. Slavich, Precise determination of the neutral Higgs boson masses in the MSSM, J. High Energy Phys. 09 (2004) 044; S. P. Martin, Three-loop corrections to the lightest Higgs scalar boson mass in supersymmetry, Phys. Rev. D **75**, 055005 (2007); R. V. Harlander, P. Kant, L. Mihaila, and M. Steinhauser, Higgs Boson Mass in Supersymmetry to Three Loops, Phys. Rev. Lett. **100**, 191602 (2008); Erratum: Higgs Boson Mass in Supersymmetry to Three Loops, Phys. Rev. Lett. **101**, 039901(E) (2008); S. Heinemeyer, O. Stal, and G. Weiglein, Interpreting the LHC Higgs search results in the MSSM,

Phys. Lett. B **710**, 201 (2012); A. Arbey, M. Battaglia, A. Djouadi, and F. Mahmoudi, Interpreting the LHC Higgs Search Results in the MSSM, J. High Energy Phys. 09 (2012) 107; The Higgs sector of the phenomenological MSSM in the light of the Higgs boson discovery, J. High Energy Phys. 09 (2012) 107.

[31] ATLAS and CMS Collaborations, Report No. ATLAS-CONF-2015-044.

[32] Y. Amhis *et al.* (Heavy Flavor Averaging Group Collaboration), Averages of b-hadron, c-hadron, and τ-lepton properties as of summer 2014, arXiv:1412.7515.

[33] K. Kowalska, L. Roszkowski, E. M. Sessolo, and A. J. Williams, GUT-inspired SUSY and the muon g − 2 anomaly: prospects for LHC 14 TeV, J. High Energy Phys. 06 (2015) 020.

[34] P. A. R. Ade *et al.* (Planck Collaboration), Planck 2013 results. XVI. Cosmological parameters, Astron. Astrophys. **571**, A16 (2014); see also G. Hinshaw *et al.* (WMAP Collaboration), Nine-year Wilkinson microwave anisotropy probe (WMAP) observations: Cosmological parameter results, Astrophys. J. Suppl. Ser. **208**, 19 (2013).

[35] D. S. Akerib *et al.* (LUX Collaboration), First Results from the LUX Dark Matter Experiment at the Sanford Underground Research Facility, Phys. Rev. Lett. **112**, 091303 (2014).

[36] A. Djouadi *et al.* (MSSM Working Group Collaboration), The minimal supersymmetric standard model: Group summary report, arXiv:hep-ph/9901246.

[37] S. Alekhin, A. Djouadi, and S. Moch, The top quark and Higgs boson masses and the stability of the electroweak vacuum, Phys. Lett. B **716**, 214 (2012).

[38] A. Djouadi, J. L. Kneur, and G. Moultaka, SuSpect: A Fortran code for the supersymmetric and Higgs particle spectrum in the MSSM, Comput. Phys. Commun. **176**, 426 (2007).

[39] G. Belanger, F. Boudjema, A. Pukhov, and A. Semenov, micrOMEGAs$_3$: A program for calculating dark matter observables, Comput. Phys. Commun. **185**, 960 (2014).

[40] A. Djouadi, J. Kalinowski, and M. Spira, HDECAY: A Program for Higgs boson decays in the standard model and its supersymmetric extension, Comput. Phys. Commun. **108**, 56 (1998).

[41] R. V. Harlander, S. Liebler, and H. Mantler, SusHi: A program for the calculation of Higgs production in gluon fusion and bottom-quark annihilation in the Standard Model and the MSSM, Comput. Phys. Commun. **184**, 1605 (2013); R. V. Harlander and W. B. Kilgore, Next-to-Next-to-Leading Order Higgs Production at Hadron Colliders, Phys. Rev. Lett. **88**, 201801 (2002); Higgs boson production in bottom quark fusion at next-to-next-to leading order, Phys. Rev. D **68**, 013001 (2003); U. Aglietti, R. Bonciani, G. Degrassi, and A. Vicini, Two loop light fermion contribution to Higgs production and decays, Phys. Lett. B **595**, 432 (2004); G. Degrassi and P. Slavich, NLO QCD bottom corrections to Higgs boson production in the MSSM, J. High Energy Phys. 11 (2010) 044; G. Degrassi, S. Di Vita, and P. Slavich, NLO QCD corrections to pseudoscalar Higgs production in the MSSM, J. High Energy Phys. 08 (2011) 128; R. Harlander and P. Kant, Higgs production and decay: Analytic results at next-to-leading order QCD, J. High Energy Phys. 12 (2005) 015.

[42] K. A. Olive *et al.* (Particle Data Group Collaboration), Review of Particle Physics, Chin. Phys. C **38**, 090001 (2014).

[43] J. E. Camargo-Molina, B. O'Leary, W. Porod, and F. Staub, Vevacious: A tool For finding The global minima of one-loop effective potentials with many scalars, Eur. Phys. J. C **73**, 2588 (2013).

[44] C. L. Wainwright, CosmoTransitions: Computing cosmological phase transition temperatures and bubble profiles with multiple fields, Comput. Phys. Commun. **183**, 2006 (2012).

[45] U. Chattopadhyay and A. Dey, Exploring MSSM for charge and color breaking and other constraints in the Context of Higgs@125 GeV, J. High Energy Phys. 11 (2014) 161.

[46] G. Aad *et al.* (ATLAS Collaboration), Search for charged Higgs bosons decaying via $H^{\pm} \to \tau^{\pm}\nu$ in fully hadronic final states using pp collision data at $\sqrt{s} = 8$ TeV with the ATLAS detector, J. High Energy Phys. 03 (2015) 088.

[47] CMS Collaboration, Report No. CMS-PAS-HIG-13-026.

[48] S. Bertolini, F. Borzumati, and A. Masiero, QCD Enhancement of Radiative B Decays, Phys. Rev. Lett. **59**, 180 (1987); N. G. Deshpande, P. Lo, J. Trampetic, G. Eilam, and P. Singer, Prediction of $B \to K^{*\gamma}$ as a Test of the Standard Model, Phys. Rev. Lett. **59**, 183 (1987); B. Grinstein and M. B. Wise, Weak radiative B meson decay as a probe of the Higgs sector, Phys. Lett. B **201**, 274 (1988); B. Grinstein, R. P. Springer, and M. B. Wise, Effective Hamiltonian for weak radiative B meson decay, Phys. Lett. B **202**, 138 (1988); W.-S. Hou and R. S. Willey, Effects of charged Higgs bosons on the processes $b \to s\gamma$, $b \to sg^*$ and $b \to s\ell^+\ell^-$, Phys. Lett. B **202**, 591 (1988); B. Grinstein, R. P. Springer, and M. B. Wise, Strong interaction effects in weak radiating anti-B meson decay, Nucl. Phys. **B339**, 269 (1990).

[49] S. Bertolini, F. Borzumati, A. Masiero, and G. Ridolfi, Effects of supergravity induced electroweak breaking on rare B decays and mixings, Nucl. Phys. **B353**, 591 (1991); R. Barbieri and G. F. Giudice, $b \to s\gamma$ decay and supersymmetry, Phys. Lett. B **309**, 86 (1993); R. Garisto and J. N. Ng, Supersymmetric $b \to s$ gamma with large chargino contributions, Phys. Lett. B **315**, 372 (1993); P. Nath and R. L. Arnowitt, $b \to s$ gamma decay in supergravity grand unification and dark matter, Phys. Lett. B **336**, 395 (1994); M. Ciuchini, G. Degrassi, P. Gambino, and G. F. Giudice, Next-to-leading QCD corrections to $B \to X_s\gamma$ in supersymmetry, Nucl. Phys. **B534**, 3 (1998); see also Ref. [55].

[50] M. S. Carena, D. Garcia, U. Nierste, and C. E. M. Wagner, $b \to s\gamma$ and supersymmetry with large $\tan\beta$, Phys. Lett. B **499**, 141 (2001).

[51] M. Carena, D. Garcia, U. Nierste, and C. E. M. Wagner, Effective Lagrangian for the $\bar{t}bH^+$ interaction in the MSSM and charged Higgs phenomenology, Nucl. Phys. **B577**, 88 (2000).

[52] A. Anandakrishnan, B. C. Bryant, and S. Raby, Threshold corrections to the bottom quark mass revisited, J. High Energy Phys. 05 (2015) 088.

[53] M. Carena, M. Olechowski, S. Pokorski, and C. E. M. Wagner, Electroweak symmetry breaking and bottom-top Yukawa unification, Nucl. Phys. **B426**, 269 (1994).

[54] U. Haisch and F. Mahmoudi, MSSM: Cornered and correlated, J. High Energy Phys. 01 (2013) 061.

[55] G. Degrassi, P. Gambino, and G. F. Giudice, $B \to X_s\gamma$ in supersymmetry: Large contributions beyond the leading order, J. High Energy Phys. 12 (2000) 009.

[56] R. Aaij *et al.* (LHCb Collaboration), Measurement of the $B_s^0 \to \mu^+\mu^-$ Branching Fraction and Search for $B^0 \to \mu^+\mu^-$ Decays at the LHCb Experiment, Phys. Rev. Lett. **111**, 101805 (2013).

[57] S. Chatrchyan *et al.* (CMS Collaboration), Measurement of the $B_s^0 \to \mu^+\mu^-$ Branching Faction and Search for $B^0 \to \mu + \mu-$ with the CMS Experiment, Phys. Rev. Lett. **111**, 101804 (2013).

[58] V. Khachatryan *et al.* (CMS Collaboration), Search for disappearing tracks in proton-proton collisions at $\sqrt{s} = 8$ TeV, J. High Energy Phys. 01 (2015) 096; G. Aad *et al.* (ATLAS Collaboration), Search for charginos nearly mass degenerate with the lightest neutralino based on a disappearing-track signature in pp collisions at $\sqrt{s} =$ 8 TeV with the ATLAS detector, Phys. Rev. D **88**, 112006.

[59] M. Chakraborti, U. Chattopadhyay, S. Rao, and D. P. Roy, Higgsino dark matter in nonuniversal gaugino mass models, Phys. Rev. D **91**, 035022 (2015), and references therein.

[60] G. Aad *et al.* (ATLAS Collaboration), Expected performance of the ATLAS experiment: Detector, trigger and physics, arXiv:0901.0512.

[61] A. Elagin, P. Murat, A. Pranko, and A. Safonov, A new mass reconstruction technique for resonances decaying to $\tau\tau$, Nucl. Instrum. Methods Phys. Res., Sect. A **654**, 481 (2011).

[62] J. Alwall, R. Frederix, S. Frixione, V. Hirschi, F. Maltoni, O. Mattelaer, H.-S. Shao, T. Stelzer, P. Torrielli, and M. Zaro, The automated computation of tree-level and next-to-leading order differential cross sections, and their matching to parton shower simulations, J. High Energy Phys. 07 (2014) 079.

[63] T. Sjostrand, S. Mrenna, and P. Z. Skands, PYTHIA 6.4 Physics and Manual, J. High Energy Phys. 05 (2006) 026.

[64] ATLAS Collaboration, Reports No. ATL-PHYS-PUB-2009-088, No. ATL-COM-PHYS-2009-345.

[65] M. Cacciari, G. P. Salam, and G. Soyez, FastJet User Manual, Eur. Phys. J. C **72**, 1896 (2012).

[66] L. J. Hall, R. Rattazzi, and U. Sarid, Top quark mass in supersymmetric SO(10) unification, Phys. Rev. D **50**, 7048 (1994).

[67] J. Guasch, P. Hafliger, and M. Spira, MSSM Higgs decays to bottom quark pairs revisited, Phys. Rev. D **68**, 115001 (2003).

[68] S. Dawson, C. B. Jackson, and P. Jaiswal, SUSY QCD corrections to Higgs-b production: Is the Δ_b approximation accurate?, Phys. Rev. D **83**, 115007 (2011).

[69] T. Plehn, G. P. Salam, and M. Spannowsky, Fat Jets for a Light Higgs, Phys. Rev. Lett. **104**, 111801 (2010).

[70] A. Cakir (CMS and ATLAS Collaborations), Prospects of new physics searches using High Lumi-LHC, arXiv: 1412.8503.